Computers and Chemical Engineering 97 (2017) 161–174

Contents lists available at ScienceDirect

Computers and Chemical Engineering

journal homepage: www.elsevier.com/locate/compchemeng

A parametric evaluation of powder flowability using a Freeman rheometer through statistical and sensitivity analysis: A discrete element method (DEM) study

S.K. Wilkinson*, S.A. Turnbull, Z. Yan, E.H. Stitt, M. Marigo

Johnson Matthey Technology Centre, Billingham, PO Box 1, TS23 1LB, UK

ARTICLE INFO

Article history:
Received 1 April 2016
Received in revised form
23 November 2016
Accepted 29 November 2016
Available online 1 December 2016

Keywords:
Discrete element method
Freeman rheometer
Flowability
Particle properties
Parameter estimation
Principal component analysis

ABSTRACT

The flowability of powders in a Freeman Rheometer (FT4) is explored in this study using discrete element method (DEM). Five DEM input parameters describing particle properties: static and rolling friction coefficients, coefficient of restitution, Young's modulus and cohesion energy density (using JKR cohesion model) were explored in a matrix of simulations using Design of Simulation (DoS) principles. The impact of these parameters was assessed against two responses from the FT4 test: the basic flowability energy (BFE) and specific energy (SE). By using a combination of empirical effects and interactions analysis and principal component analysis (PCA), it was found that static and rolling friction parameters play a critical role in determining the BFE and SE of a powder, whilst cohesion energy density also plays a significant role in influencing BFE. The combination of these methods has helped deliver a roadmap to show which parameters would be effectively calibrated on an FT4.

1. Introduction

Flowability is the ability of granular media and powders to flow under specific stress and flow rate conditions (Mort et al., 2015), and can influence process performance during powder handling, including hopper discharge, powder feeding, blending, mixing, and die filling. Additionally, this can influence product quality. Flowability depends on multiple physical properties (for example: particle size, particle size distribution, shape factors, and surface texture) and environmental variables (temperature, humidity, pressure, etc.) (Ganesan et al., 2008; Yang and Evans, 2007). The development of experimental and/or modelling techniques to predict flowability of powders and granular media is therefore a critical precursor in optimising process performance.

In recent years there has been an increase in the application of Discrete Element Method (DEM), originated by Cundall and Strack, to study properties such as flowability of granular media and powders *in silico* (Cundall and Strack, 1979). DEM is based on the description of the microscopic contacts between a number of discrete particles. The importance of DEM has been investigated in different fields such as chemical engineering, pharmaceuticals, powder metallurgy, agriculture and many others. DEM simulations have been extensively applied to diverse problems in powder handling processes such as packing of particles (Matuttis et al., 2000; Zhang et al., 2001; Dutt et al., 2005), flow from a hopper (Cleary and Sawley, 2003; Anand et al., 2008; Ketterhagen et al., 2009), die filling (Wu, 2008; Guo et al., 2010), fragmentation of agglomerates (Thornton et al., 1996; Liu et al., 2010), bulk compression (Martin and Bouvard, 2003; Samimi et al., 2005; Hassanpour and Ghadiri, 2004; Markauskas and Kacianauskas, 2006), flow in a screw conveyor (Moysey and Thompson, 2005; Owen and Cleary, 2009) and powder mixing (Anand et al., 2008; Yang et al., 2008; Marigo et al., 2010; Alizadeh et al., 2014).

The reliability of a DEM model is strongly dependent on the accuracy of the contact model and the particle property parameters chosen as inputs to the simulation (Benvenuti et al., 2016). The choice of DEM input parameters is still a key limitation and an aspect of controversy for the effective application of this modelling tool (Marigo and Stitt, 2015). The parameters are often chosen based on bulk powder properties, rather than measured behaviour of a single particle. A very common practice is to calibrate the DEM model against bulk global measurements and adjust input parameters until the model outputs match experimental observations (Marigo and Stitt, 2015).

* Corresponding author.
E-mail address: sam.wilkinson@matthey.com (S.K. Wilkinson).

http://dx.doi.org/10.1016/j.compchemeng.2016.11.034
0098-1354/

Nomenclature

Symbol

a	Number of principal components
A	Particle contact area m^2
C	Stiffness term
D_{ij}	Distance between particles i and j m
E	Energy J
err	Error
F	Force Pa
G	Shear modulus Pa
G^*	Equivalent shear modulus Pa
h	Depth of the blade in the powder bed m
$(J)_{np}$	Norm of the Jacobian matrix
k	Cohesion energy density J m^{-3}
m	Mass kg
m^*	Equivalent mass kg
n_p	Number of parameters
n_{sim}	Number of simulations
$\boldsymbol{P}$	Loadings (in PCA)
Par	Fitting parameter
$\boldsymbol{Q}$	Scores (in PCA)
R	Radius of particle m
R^*	Equivalent radius of particles m
$S(\beta)$	Residual sum of squares for model of comprising β parameters
$\hat{t}_{ij}$	Tangential unit vector term
T	Torque Pa
T_R	Critical time step s
v	Velocity m s^{-1}
W	Work J
Y	Young's modulus Pa
Y^*	Equivalent Young's modulus Pa
y_i	Model output response varies

Greek letters

α	Helix angle
β	DEM simulation input parameter varies
δ	Interparticle overlap m
ε	Coefficient of restitution
μ_r	Rolling friction coefficient
μ_s	Static friction coefficient
ξ	Input variable varies
ρ	Density kg m^{-3}
σ_y	Yield stress Pa
ψ	Damping ratio coefficient

Subscripts

coh	Of cohesion
$high$	High position in DoS
ij	Between particle i and j
low	Low position in DoS
n	Normal
pp	Particle-particle
pw	Particle-wall
t	Tangential

Superscripts

t	Transpose

Acronym

AFM	Atomic force microscopy
BFE	Basic flowability energy
DEM	Discrete element method
DoE	Design of experiments
DoS	Design of simulations
EPSD	Elastic-plastic-spring-dashpot
FT4	Freeman FT4 rheometer
PCA	Principal component analysis
PLS	Partial least squares
SE	Specific energy

Obtaining measured values for these inputs parameters is challenging and time consuming, as measurements require consideration of individual particles. A few attempts have been made to measure some input parameters including, Young's modulus (Y) of single particles (Leisena et al., 2012; Marigo et al., 2014), the yield stress (σ_y) (Prabhu, 2005) and interfacial energy using Atomic Force Microscopy (AFM) (Jones, 2003; Davies et al., 2005).

Even if single particle contact properties could be measured there is a major challenge due to the mismatch of scales between the contact model (single particle interactions) and the input parameters. Due to computational costs, the particle size employed in the simulations is often artificially enlarged by the use of techniques such as coarse graining (Radl et al., 2011; Nasato et al., 2015). As a consequence, particle contact parameters need to be readjusted to account for the different sizes. For example, in Thakur et al., 2015; a methodology was proposed for the scaling of model parameters to produce scale independent predictions for cohesive and non-cohesive solids under a quasi-static simulation of confined compression and unconfined compression to failure in a uniaxial test. The presented methodology only involved particles between 2.75 and 3 mm and did not present results for finer particles or compare with experimental data.

The literature shows a number of approaches which are aimed at developing effective calibration tools for DEM and ultimately our practical understanding of powder flow. A variety of approaches to understanding the global impact of input parameters on a DEM simulation have been used elsewhere in the literature for different applications. In the study of flow from hoppers, Liu et al. (2014) looked at the impact of particle aspect ratio on the DEM simulation output and compared with experiments. This parameter had a strong impact on discharge rate and the simulations allowed the authors to develop a modified description of the classic Beverloo equation. It is possible however, that such an approach may only be constrained to a narrow window as particle properties such as $\mu_{r,pp}$ and $\mu_{s,pp}$ were not varied. Zhou *et al.* (2002) did look at the impact of $\mu_{r,pp}$ and $\mu_{s,pp}$ as well as particle-wall $\mu_{r,pw}$ and $\mu_{s,pw}$ on the angle of repose of a sandpile test. A power law relationship was constructed between measured angle of repose and the input parameters. All friction coefficients followed a positive dependency, with significance order $\mu_{s,pp} > \mu_{s,pw} > \mu_{r,pw} > \mu_{r,pp}$. Particle size followed a significant negative dependency. Recently, Yan et al. (2015) used a multi-level statistical analysis approach to understand the impact of $\mu_{s,pp}$, $\mu_{r,pp}$, Y and particle-particle coefficient of restitution (ε_p) on hopper flow in DEM simulations. The empirical power-law approach was found to agree with a semi-empirical which compared angle of repose to contact model parameter sensitivity matrices using principal component analysis (PCA). A further comparison with a mechanistic approach, comparing contact model outputs to contact model parameter sensitivity matrices also showed agreement. $\mu_{s,pp}$ was found to be the critical

parameter in all cases, allowing the gap to be bridged between bulk and particle-particle interactions.

Elsewhere, Remy et al. (2010) compared experiments and simulations to identify critical parameters influencing the behaviour of cohesionless particles in a bladed mixer. $\mu_{s,pp}$ was again influential, positively influencing radial and vertical velocities of particles. Höhner et al. (2013) explored different particle shapes in influencing dynamic angle of repose in a rotating drum. Simons et al. (2015) looked at the impact of parameters on an agitated mixer by coupling with a ring shear cell test as a calibration experiment. Critical parameters influencing tangential shear stress were Y (positive log-linear dependency), $\mu_{s,pp}$ (positive, non-linear; 0.1–0.3 again the key sensitivity region) and $\mu_{r,pp}$ (positive linear relationship). A similar approach was used by Grima and Wypych (2011). Freireich et al. (2009) carried out a sensitivity analysis on collision scale behaviour and found that macroscopic observations (solid faction, velocity field) do not provide a validation of collision scale behaviour.

Boukouvala et al. (2013) critically assessed the importance of parameters in DEM using a reduced-order approach. Here, PCA coupled with surrogate models mapping identified key areas of sensitivity within a DEM simulation. Only the key principal components would be retained allowing a reduced, and computationally more efficient, model to be retained for future simulations. Statistical design of experiments (DoE) has also been used to provide a more efficient approach to investigating roller compaction (Souihi et al., 2013). This comprised the use of a reduced central composite face-centered design whose results were analysed using orthogonal partial least squares (PLS) regression. Such an approach has not been used for DEM simulations, but could be highly useful in developing more universal models for particle flow in a more efficient manner.

Additionally, an artificial neural networks (ANN) approach was carried out by Benvenuti et al. (2016). Here a small matrix of simulations using different particle property input parameters were carried out using a DEM shear cell simulation to train a feed forward ANN. This provided an understanding of the impact of these parameters on the system which was then utilised to forecast the prediction of a large number of additional DEM shear cell simulations. This provided sets of possible parameter combinations which could describe the particle properties of the materials used. The number of parameter combinations was a small fraction of the original matrix of combinations. Combining with another ANN trained by sandpile simulations allows for intersection of a valid particle properties.

Bharadwaj et al. (2010) investigated the FT4 Powder Rheometer (Freeman Technology, Malvern, UK; hereby referred to as FT4) and specifically varied a number of input parameters in the DEM simulations including particle size (mean, distribution), $\mu_{r,pp}$, $\mu_{r,pp}$ and aspect ratio. Increasing the values of the latter two parameters had the greatest impact, significantly increasing force and torque measurements. A recent work by Hare et al. (2015) found that the DEM simulation under-predicted flow energies in comparison to the experiments, although the disparity reduced at high $\mu_{r,pp}$. Again, the authors found $\mu_{s,pp}$ to be a sensitive parameter on the predicted total flow energy, following a positive but non-linear trend with significant changes in the 0.1–0.3 range.

Recently, the FT4 has become an increasingly popular device for comparatively studying the flowability of particulate materials by means of measuring the flow energy. Measuring flow energy consists of a dynamic test regime, in which the flow resistance encountered for an impeller moving within a powder bed is assessed. The downward dynamic test on the FT4 provides a measure of basic flowability energy (BFE), whilst the upward dynamic test provides a measure of specific energy (SE). The FT4 has been used for comparative studies and ranking of powder flow properties. Freeman (2007) compared the flow properties of 6 powders in consolidated, conditioned and aerated state using the FT4 and a shear cell. The FT4 has potential for use as a quantitative support tool for process design or a possible calibration tool for DEM simulations, although such a practice has not yet been extensively implemented (Pantaleev et al., 2015).

The investigation of the effect of single particle properties using DEM has strong potential to act as a starting point to understand the sensitivities of powder properties on FT4 data outputs. Such an understanding could lead to a 'roadmap' of behavioural trends observed on the FT4 in the real experiment for different powder samples. This paper will focus on the use of the FT4 with the following aims:

- Understand the impact of particle property input parameters on measured flowability energies using DEM simulations of the FT4.
- Recommend an approach that achieves the above understanding with an efficient number of simulations.
- Recommend statistical and sensitivity analysis tools which can be combined to deliver a robust understanding of the impact of input parameters on the FT4 simulation.
- Discuss where understanding from FT4 simulations in DEM can act as a (qualitative) roadmap and calibration tool for observations in experimental FT4 tests based on chosen powder properties the user wishes to measure.

2. Methodologies

2.1. Discrete element method (DEM)

The DEM employed in this work uses the soft-sphere approach originally developed by Cundall and Strack, (1979). This method is based on Newton's equations of motion of individual particles. In this work, the Hertz-Mindlin contact model is utilised (Hertz, 1881; Mindlin, 1949). The normal forces, F_{ij}^n on each sphere is given by:

$$F_{ij}^n = -\frac{4}{3}Y^*\sqrt{R^*}\delta_{ij}^{n3/2} - 2\sqrt{\frac{5}{6}}\psi\sqrt{C_n m^*}v_{ij}^n \quad (1)$$

where E^* is the equivalent Young's Modulus of the two colliding particles, defined by $\frac{1}{Y_*} = \frac{1-\nu_i^2}{Y_i} + \frac{1-\nu_j^2}{Y_j}$, where ν_i and ν_j are the Poisson's ratios; R^* is the equivalent radius, defined by $\frac{1}{R_*} = \frac{1}{R_i} + \frac{1}{R_j}$; m^* is the equivalent mass, defined by $\frac{1}{m_*} = \frac{1}{m_i} + \frac{1}{m_j}$; v_{ij}^n and $v_{ij}^t\delta_{ij}^n$ is the normal contact overlap, given by $|\delta_{ij}^n| = R_i + R_j - d_{ij}$, where d_{ij} is the distance of the centre of colliding particles; δ_{ij}^t is tangential contact overlap, given by the integral of the tangential relative velocity through the collision time since the collision starts, i.e., $|\delta_{ij}^t| = \int_0^t |v_{ij}^t| dt$; $C_n = 2E^*\sqrt{R^*\delta_{ij}^n}$ and $C_t = 8G^*\sqrt{R^*\delta_{ij}^n}$ are the normal and tangential contact stiffness; ψ is the damping ratio coefficient which is a function of the coefficient of restitution, ε, given by $\psi = \ln(\varepsilon)/\sqrt{\ln^2(\varepsilon) + \pi^2}$.

Tangential force F_{ij}^t is given by:

$$F_{ij}^t = \min\{-8G^*\sqrt{R^*\delta_{ij}^n}\delta_{ij}^t - 2\sqrt{\frac{5}{6}}\psi\sqrt{C_t m^*}, -\mu_s|F_{ij}^t|\hat{t}_{ij}\} \quad (2)$$

where $C_t = 8G^*\sqrt{R^*\delta_{ij}^n}$ is tangential contact stiffness, G^* is the equivalent shear modulus, defined by $1/G^* = 1/G_i + 1/G_j$; v_{ij}^t is the tangential component velocity at the contact, δ_{ij}^t is the tangential overlap at the contact. The term $\hat{t}_{ij}$ is the tangential unit vector term.

Rotation of particle is accounted by rolling torque$T$

$$T = -\mu_r |F_n| \frac{\omega}{|\omega|} \tag{3}$$

Cohesion of particles is modelled with the Johnson-Kendall-Roberts model – JKR model (Johnson et al., 1971). An additional term $\boldsymbol{F}_{\text{coh}}$ is added to Eq. (3). The $\boldsymbol{F}_{\text{coh}}$ is given by:

$$\text{F}_{\text{coh}} = \text{kA} \tag{4}$$

where A is the particle contact area; $\boldsymbol{k}$ is the cohesion energy density in J m^{-3}, contact area A is calculated as Eq. (5):

$$A = 2\pi\delta_{ij}^{n}(2R^{*}) \tag{5}$$

In this work the time step Δt has been selected equal to 10% of the critical time step T_R. T_R was evaluated from the equation proposed by Thornton and Randall, (1988). The critical time-step is determined from the Rayleigh wave propagating on the surface of the smallest sphere:

$$\Delta t < T_R = \frac{\pi R\sqrt{\rho/G}}{0.01631\,\nu + 0.8766} \tag{6}$$

2.2. Design of Simulation (DoS) methods

Traditionally, experiments and simulations are often carried out using a "one-at-a-time" type approach, whereby one parameter is varied, and the others are kept constant, to establish the effect of that parameter. This is not only very time and resource consuming due to the increased number of experiments; it also does not completely cover the experimental space, thus resulting in a sub-optimal solution, and lack of information regarding interactions between the different parameters.

A design of experiments (DoE) approach covers all of the experimental space using only a few experimental points, maximising orthogonal variance, and thus producing a robust dataset for multivariate analysis. This in turn allows assessment of interactions between parameters and their effects on the experimental output. The general notation for DoE giving the number of required experiments is L^{x-n}, where L is the number of levels, commonly 2, x is the number of variables, and n is an optional fractional reduction.

In this specific case, the experiments are replaced by simulated tests, and thus this methodology shall be more accurately referred to as "design of simulations" (DoS). This DoS approach was used herein to produce a small matrix of simulations required to fully "map" the experimental space, using both full (2^{x}) and fractional factorial (2^{x-n}) designs in order to demonstrate the power of DoS to reduce the number of tests required. The DoS matrices and subsequent main effect and interactions analyses were completed using Unscrambler® X 10.3 (CAMO Software AS, Oslo, Norway).[1]

2.3. Statistical and sensitivity analysis techniques

2.3.1. Parameter estimation methods

Parameter estimation was carried out using Athena Visual Studio v14.2© software.[2] All models tested using parameter estimation methods in this study were explicit in nature and of the single response type. The parameter estimation method used was a Bayesian estimation method with an objective function to minimise the residual sum of squares ($S(\beta)$):

$$y_i = f_i\left(\xi_i, \beta\right) + err \tag{7}$$

where ξ_i denotes the independent variables for associated with each simulation observation (y_i), β the parameters in the model and err the independent random error in the observations. An assumption for this approach is that the error distributions in the observations are normally distributed. As the results presented in this paper are simulation outputs, the error in observations should be zero and each observation completely reproducible. This therefore allows the objective function to be treated purely on a model inadequacy basis, rather than a combination of model inadequacy and observation error. This aspect is checked in Section 3.3.

2.3.2. Parameter sensitivity analysis and model reduction

The methodology described in this section aims to calculate a ranking of model parameters in order of sensitivity with respect to model responses. This is based on methodologies used in Quiney and Schuurman, (2007) and Wilkinson et al. (2015) which sequentially eliminate the least sensitive parameters in the model. For each time a parameter is removed, the statistical impact on the predictive outputs of the model is assessed.

This form of analysis begins with the Jacobian matrix, J, of size $n_{sim} \times n_p$, where n_{sim} is the total number of *completed* simulations in the simulation design where the output responses are known and n_p is the number of model parameters. Each model parameter has a set of i sensitivities associated with it, where $i = n_p$. This set is processed into a form known as the norm of the Jacobian matrix:

$$norm\ \ (\boldsymbol{J})_{np} = \sqrt{\sum_{i}\left(\beta_{np}\frac{dy_i}{d\beta_{np}}\right)^{2}} \tag{8}$$

where $norm(\boldsymbol{J})_{np}$ denotes the norm of the parameter sensitivity matrix and is calculated for each parameter in the model. In effect this method provides a summated representation of the sensitivities for a particular parameter in the dataset. Each sensitivity value is scaled by the value of the parameter itself as a normalisation technique. The magnitude of each of the $norm(\boldsymbol{J})_{np}$ values can be compared. The smallest $norm(\boldsymbol{J})_{np}$ corresponds to the least influential parameter in the model.

Each time a parameter is removed from a model, the remaining parameters are re-estimated using the model in its reduced $(n_p - 1)$ form. The statistical impact on the residuals of the fit, $S(\beta)$, can be understood via use of the F-test:

$$F = \frac{\left(\frac{S(\beta)_1 - S(\beta)_2}{\beta_2 - \beta_1}\right)}{\left(\frac{S(\beta)_2}{i - \beta_2}\right)} \tag{9}$$

where F denotes the F-statistic and subscripts 1 and 2 relate to the model containing $(n_p\text{-}1)$ and n_p parameters respectively. The F statistic generated is compared with F_{crit} ($p = 0.05$) under these constraints. If the F-statistic is smaller than F_{crit}, the removal of the proposed parameter is deemed acceptable as a statistically significant increase in residuals has not been induced.

2.3.3. Principal component analysis (PCA)

PCA is an exploratory data analysis technique, developed by Pearson in 1901, and popularised in the 1960–80 s with the increase in computing power available (Pearson, 1901; Jolliffe, 2002). Since then PCA has been a popular and powerful tool for analysing highly dimensional data.

The technique essentially compresses a large dataset (ξ variables by n_{sim} samples) down into a smaller number (a) of underlying correlations or Principal Components (PCs). The number of PCs ideally describes the number of significant components in the system, with each PC being comprised of scores ($\boldsymbol{Q}$) and loadings ($\boldsymbol{P}$). The scores describe the magnitudes of the new compressed variables, representing the relationships between the samples. The loadings are the

[1] The Unscrambler ® X 10.3, CAMO Software AS, Oslo, Norway.
[2] Athena Visual Workbench 14.2, Stewart & Associates Engineering Software, Inc.

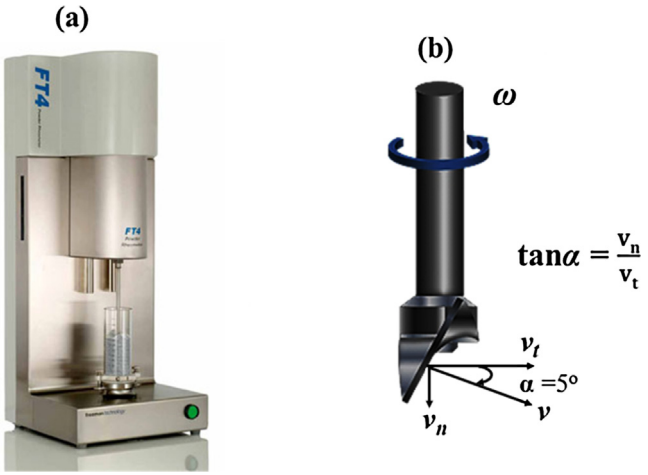

Fig. 1. FT4: (a) instrument; (b) impeller, where α is the helix angle, v is the blade tip speed, v_n is the axial velocity of the blade, v_t is rotational velocity (Source: Freeman Technology).

new "definitions" of the new underlying variables with respect to the original variables, representing the relationships between the original variables. The PCA decomposition is described below in Eq. (10):

$$X = \boldsymbol{TQ}^{\boldsymbol{t}} + \boldsymbol{Z} \tag{10}$$

where $\boldsymbol{T}$ is the n_{sim} by a scores matrix for the a PCs, $\boldsymbol{Q}^t$ is the transpose of the ξ by a loadings matrix, and E is the ξ by n_{sim} residuals matrix.

Thus, the PCs describe the underlying, multivariate relationships between the variables and samples, and can show how these variables vary with respect to each other (i.e. how correlated/anti-correlated they are), or how samples differ, or change over time in the case of on-line experimental or process data.

The PCA in this work was carried out using the PLS_Toolbox v8.0©[3] with MATLAB v8.5®,[4] and the Unscrambler® X.

3. DEM simulations

3.1. Simulation setup

3.1.1. Description of the FT4

The FT4 (Fig. 1A) measures the axial force and torque on the impeller (Fig. 1B) that is rotated and moved downwards and upwards through the powder bed. The force and torque reflect the resistance of powder flow, or the bulk flow properties. The more the particles resist motion and the more difficult it is to move the blade.

Total flow energy is defined by the calculation of work done that incorporates both the force and torque signals. When the blade is driven downwards through the powder bed by distance dh, rotational work increment, dW_t and axial work increment, dW_n:

$$dW_t = Td\theta = T\frac{v_t(dh/v_n)}{R} = \frac{T}{R}\frac{v_t}{v_n}dh = \frac{T}{R\tan\alpha}dh$$
$$dW_n = Fdh \tag{11}$$

where T is the torque on impeller blade, F the downward force acting on the blade (measured on base of the vessel), R the radius of the impeller and α the helix angle of impeller movement. Consequently the energy gradient the energy gradient dE is given by Eq. (12):

$$dE = dW_t + dW_n = \left(\frac{T}{R\tan\alpha} + F\right)dh \tag{12}$$

The total energy is therefore calculated by integrating the energy gradient throughout the entire blade descent through the bed.

$$E = \int_0^h \left(\frac{T}{R\tan\alpha} + F\right)dh \tag{13}$$

The energy measured during the downward and upward blade movements are the BFE and SE respectively. BFE is a measure of the powder's flowability when forced to flow, which would be encountered in processes such as through a screw feeder or in an active feed frame. SE is a measure of the powder's flowability when unconfined, which would be encountered in low stress filling, or low shear blending.

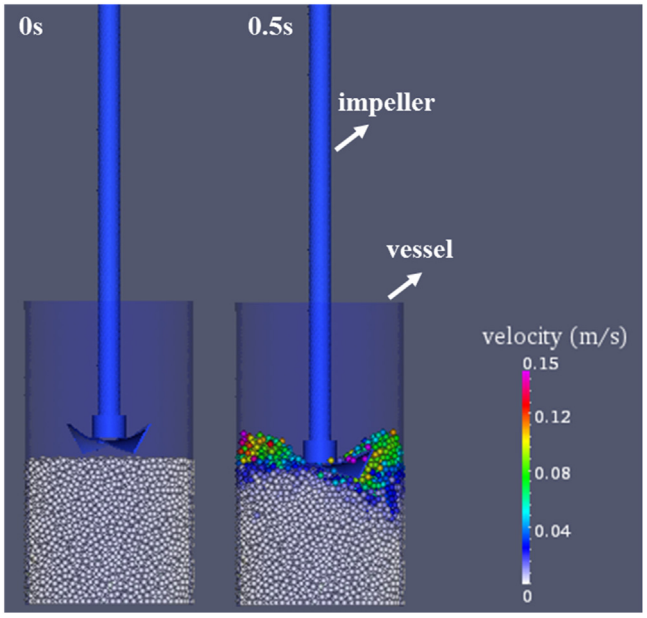

Fig. 2. DEM setup for the FT4.

3.1.2. DEM simulation procedures

A DEM simulation setup for the FT4 was established using an open source DEM code LIGGGHTS (Kloss et al., 2012). Particles were settled in a vessel (Φ = 50 mm × 90 mm) under gravity. Powder bed was conditioned by moving the impeller downwards and upwards at a helix angle of − 5° while the blade was rotated in clockwise direction with a tip speed of 100 mm s^{-1}. A powder bed with a height of 50 mm was used for simulation as shown in Fig. 2. For the BFE test, the impeller moves downwards through the powder bed in anti-clockwise direction (right) at a helix angle of 5° and with a blade tip speed of 100 mm s^{-1}. This is equivalent to an axial speed of 8.7 mm s^{-1} and a rotational speed of 4.1 rad s^{-1}.

For the SE test, the impeller moves upwards in a clockwise direction at a helix angle of −5° at a tip speed of 100 mm s^{-1}. Several tests show that the conditioning stage has almost no effect on the calculation of the energy as found in Bharadwaj et al. (2010). For the all following tests to be discussed, the conditioning step was ignored to reduce the CPU time cost. Several repeat tests have shown that the established simulation is very robust and stable.

[3] PLS_Toolbox 8.0, Eigenvector Research, Inc., USA.
[4] MATLAB 8.5, The MathWorks, Inc., UK.

Table 1
DEM input parameters fixed throughout the study.

Material parameters	Symbols	Values
Young modulus vessel (GPa)[a]	Y_v	64
Young modulus blade (GPa)[b]	Y_b	190
Poisson's ratio vessel (−)[a]	ν_v	0.25
Poisson's ratio blade (−)[b]	ν_b	0.30
Poisson's ratio particle (−)	ν_p	0.2
Particle density (kg m^{-3})	ρ	2500
Coefficient of restitution particle-blade (−)	ε_{pb}	0.7
Coefficient of restitution particle-vessel (−)	ε_{pv}	0.7
Static friction coefficient particle-blade (−)	$\mu_{s\text{-}pb}$	0.30
Static friction coefficient particle-vessel (−)	$\mu_{s\text{-}pv}$	0.30
Rolling friction coefficient particle-blade (−)[a]	$\mu_{r\text{-}pb}$	0.05
Rolling friction coefficient particle-vessel (−)[a]	$\mu_{r\text{-}pv}$	0.05
Cohesion energy density particle-blade (J m^{-3})	k_{pb}	50
Cohesion energy density particle-vessel (J m^{-3})	k_{pv}	50

[a] Bharadwaj et al. (2010).
[b] Source: Azo Materials.

3.2. DEM input parameters

3.2.1. Fixed parameters throughout the study

In the current system, the vessel is made of borosilicate glass; the impeller blade is made of SUS360 stainless steel. Some of the material properties were selected from the literature. It is known that boundary conditions such as restitution and friction between particle and walls (blade and vessel in this case) may also have an effect on the bulk particle behaviour in motion, however to reduce the number of simulations the other material and container properties were fixed as constants. These constant input parameters are listed in Table 1:

3.2.2. Parameters varied in the Design of Simulations (DoS)

In this study, five particle properties are varied as part of the DoS: Young's modulus (Y), coefficient of restitution (ε_p), static friction coefficient ($\mu_{s,pp}$) and rolling friction coefficient ($\mu_{r,pp}$), and cohesion energy density (k). The latter four parameters are properties concerning particle-particle interactions.

Table 2 lists the values of the five particle properties that are varied in this study. For each parameter, there are three values which constitute a low, centre and high position for that parameter. It is noted that in the case of ε_{pp}, $\mu_{s,pp}$ and $\mu_{r,pp}$ the centre positions are linearly spaced between the low and high values. For Y and k, the centre positions are spaced on a logarithmic scale. Using these values, three DoS matrices were generated which will form the basis for later analysis in this work:

- Full Factorial Design: $2^5 + 3 = 35$ simulations (all combinations of parameters in low and high position) plus three replicate simulations with all values in the centre position.
- Half Factorial Design: $2^{5-1} + 2 = 18$ simulations (reduced combinations of parameters in low and high position) plus two replicate simulations with all values in the centre position.
- Quarter Factorial Design: $2^{5-2} + 2 = 10$ simulations (reduced combinations of parameters in low and high position) plus two replicate simulations with all values in the centre position.

Table 2
DEM particle input parameters varied in the DoS.

Material parameters	Symbol	Values
Young modulus particles (GPa)	Y	0.02, 2.0, 200
Coefficient of restitution particle- particle (−)	ε_{pp}	0.05, 0.45, 0.85
Static friction coefficient particle-particle (−)	$\mu_{s,pp}$	0.05, 0.275, 0.50
Rolling friction coefficient particle-particle (−)	$\mu_{r,pp}$	0.05,0.25, 0.45
Cohesion energy density particle-particle (J m^{-3})	k	10, 1000, 100000

Table 3
BFE and SE measurements from the DEM simulations.

$\mu_{s,pp}$	$\mu_{r,pp}$	ε_p	Y (Pa)	k (J m^{-3})	BFE(J)	SE (J)
0.05	0.05	0.05	2.0×10^7	10	0.1255	0.0689
0.5	0.05	0.05	2.0×10^7	10	0.2734	0.1009
0.05	0.45	0.05	2.0×10^7	10	0.1690	0.0857
0.5	0.45	0.05	2.0×10^7	10	0.6503	0.1565
0.05	0.05	0.85	2.0×10^7	10	0.1241	0.0684
0.5	0.05	0.85	2.0×10^7	10	0.2809	0.1062
0.05	0.45	0.85	2.0×10^7	10	0.1687	0.0863
0.5	0.45	0.85	2.0×10^7	10	0.7511	0.1791
0.05	0.05	0.05	2.0×10^{11}	10	0.1267	0.0678
0.5	0.05	0.05	2.0×10^{11}	10	0.2692	0.1016
0.05	0.45	0.05	2.0×10^{11}	10	0.1693	0.0815
0.5	0.45	0.05	2.0×10^{11}	10	0.6373	0.1590
0.05	0.05	0.85	2.0×10^{11}	10	0.1269	0.0687
0.5	0.05	0.85	2.0×10^{11}	10	0.2778	0.1059
0.05	0.45	0.85	2.0×10^{11}	10	0.1716	0.0784
0.5	0.45	0.85	2.0×10^{11}	10	0.7648	0.1953
0.05	0.05	0.05	2.0×10^7	100000	0.1567	0.0824
0.5	0.05	0.05	2.0×10^7	100000	0.3266	0.1204
0.05	0.45	0.05	2.0×10^7	100000	0.1834	0.0937
0.5	0.45	0.05	2.0×10^7	100000	0.8379	0.1696
0.05	0.05	0.85	2.0×10^7	100000	0.1516	0.0793
0.5	0.05	0.85	2.0×10^7	100000	0.3576	0.1317
0.05	0.45	0.85	2.0×10^7	100000	0.1773	0.0912
0.5	0.45	0.85	2.0×10^7	100000	1.0687	0.2110
0.05	0.05	0.05	2.0×10^{11}	100000	0.1268	0.0671
0.5	0.05	0.05	2.0×10^{11}	100000	0.2691	0.1017
0.05	0.45	0.05	2.0×10^{11}	100000	0.1718	0.0848
0.5	0.45	0.05	2.0×10^{11}	100000	0.6127	0.1593
0.05	0.05	0.85	2.0×10^{11}	100000	0.1240	0.0664
0.5	0.05	0.85	2.0×10^{11}	100000	0.2788	0.1051
0.05	0.45	0.85	2.0×10^{11}	100000	0.1691	0.0873
0.5	0.45	0.85	2.0×10^{11}	100000	0.7232	0.1891
0.275	0.25	0.45	2.0×10^9	1000	0.4178	0.1311
0.275	0.25	0.45	2.0×10^9	1000	0.4178	0.1311
0.275	0.25	0.45	2.0×10^9	1000	0.4178	0.1311

Tables showing the simulations which appear in the full, half and quarter factorial designs can be found in Supplementary Information.

3.3. Simulation outputs

3.3.1. Force, torque and flow energy

Force and torque were recorded every 1 *ms*. Figs. 3A and 3B plot the typical force and torque on the blade for the entire test cycle including the down cycle (0–4.5 s) and the up cycle (4.5–9.0 s). Fig. 3C shows the corresponding flow energy calculated using Eq. (13). During the down cycle, the blade is rotated in anti-clockwise direction; the blade is chopping and compressing the powder bed, while the blade is lifting the powder bed in the up cycle with blade being rotated in clockwise direction. Hence, the powder shows much greater resistance during the down cycle. It is noticed that tests at high level of friction and restitution coefficient (black and red curves) show higher force and torque and flow energy than those at low levels (blue and green curves). For the same restitution coefficient and friction coefficients, highly cohesive powder shows higher flow energy (poorer flowability). But in terms of the force and torque, the effect of the cohesive energy density k is not obvious for the low level input simulations. This means study of the sensitivity of input parameters by assessing the force and torque response can be insufficient. Thus, in this study, we preferably use the flow energy (BFE for the first 4.5 s and SE for the last 4.5s) data for the parametric studies.

Table 3 reports the BFE and SE measurements under all input parameter levels corresponding to the full DoS design.

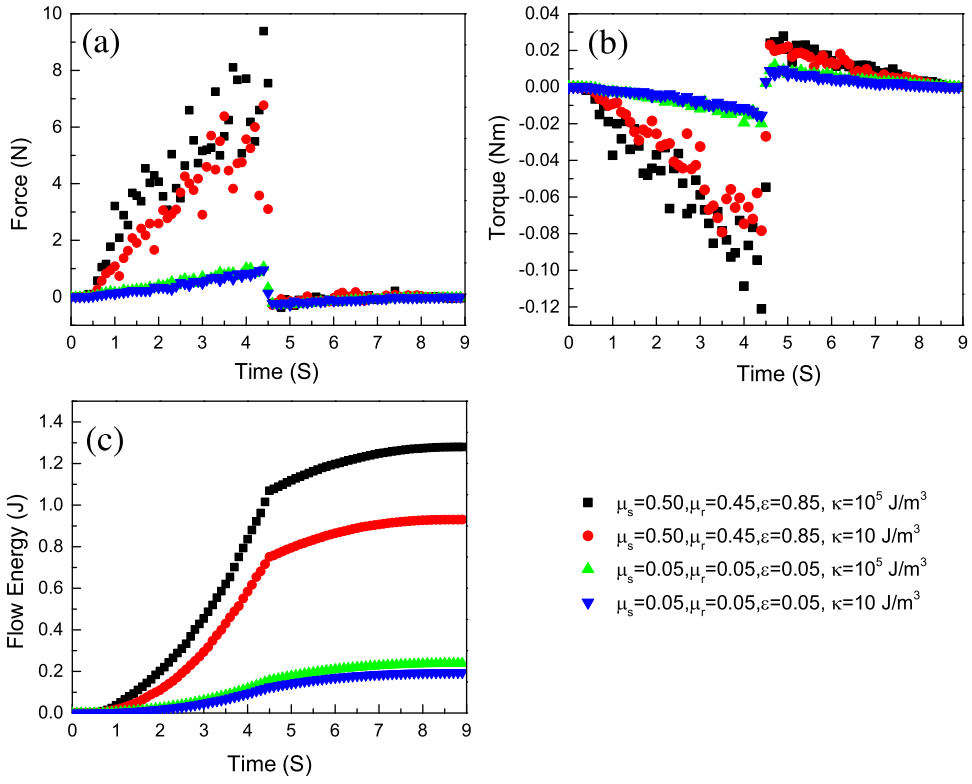

Fig. 3. Blade force, torque and flow energy during test cycle. Young's modulus Y = 2.0 × 10^7 Pa.

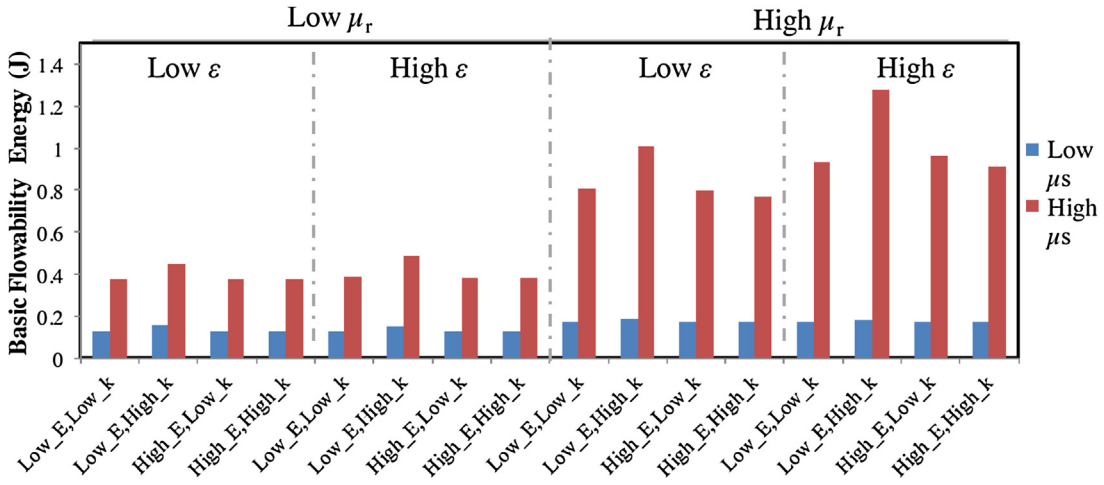

Fig. 4. Effect of friction coefficients on flow energy.

3.3.2. *Effect of static/rolling friction coefficient*

Fig. 4 shows the flow energy for powders with different input particle properties (see Table 2). From this chart, it can be seen that for the same input particle properties, high static friction coefficient (red) leads to high BFE. For the same level of static friction coefficient, higher rolling friction coefficient leads to higher BFE. It can also be seen that with an increase in the restitution coefficient, the BFE has a slight increase for the powders that have high static friction coefficient.

3.3.3. *Effect of Young's modulus*

Fig. 5 shows the effect of *Y* on the BFE. It is noticed that, in general, given the other parameters are the same, a higher *Y* leads to a higher BFE, except in the scenario when $\mu_{s,pp}$, $\mu_{r,pp}$ and *k* are all in high positions. This implies that *Y* has a negative impact on flow energy under specific conditions.

3.3.4. *Effect of restitution coefficient*

Fig. 6 shows the effect of the restitution coefficient on the flow energy measurement. It is shown that for the same other input parameters, a higher restitution coefficient results in a higher flow energy, although this is not as strong as the impact of parameters $\mu_{s,pp}$ and $\mu_{r,pp}$ It shows also for the same restitution coefficient, lower Young's modulus leads to slightly high flow energy. This implies the Young's modulus and restitution coefficient is negatively cross correlated.

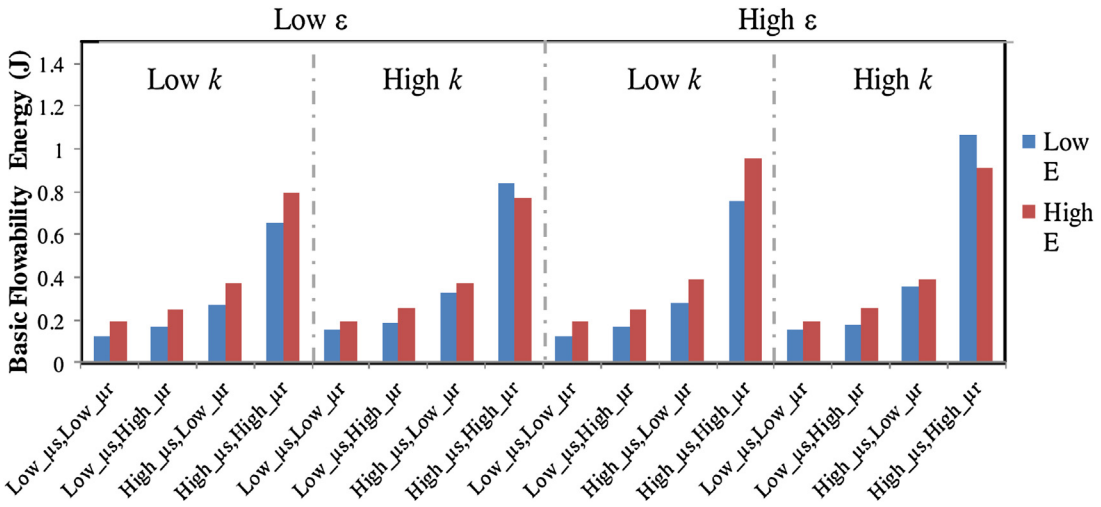

Fig. 5. Effect of Young's Modulus on flow energy.

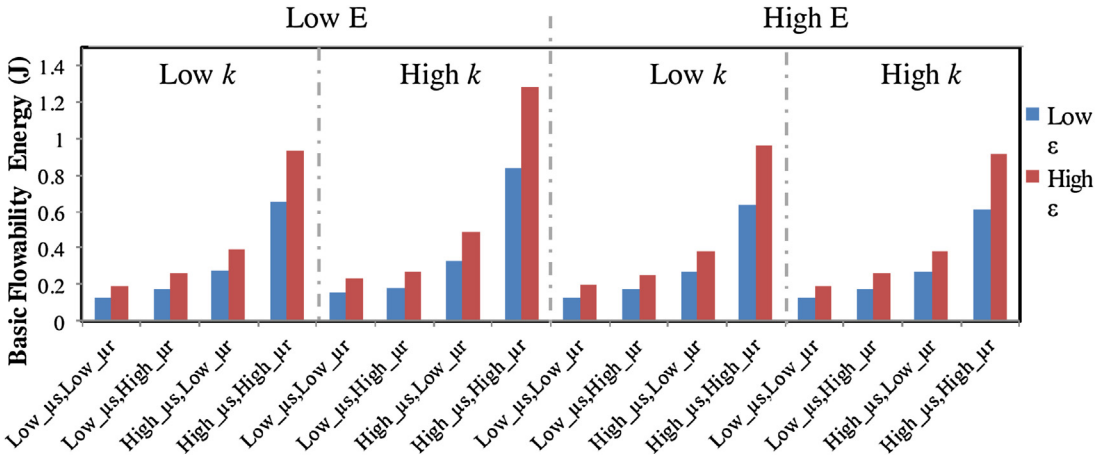

Fig. 6. Effect of restitution coefficient on flow energy.

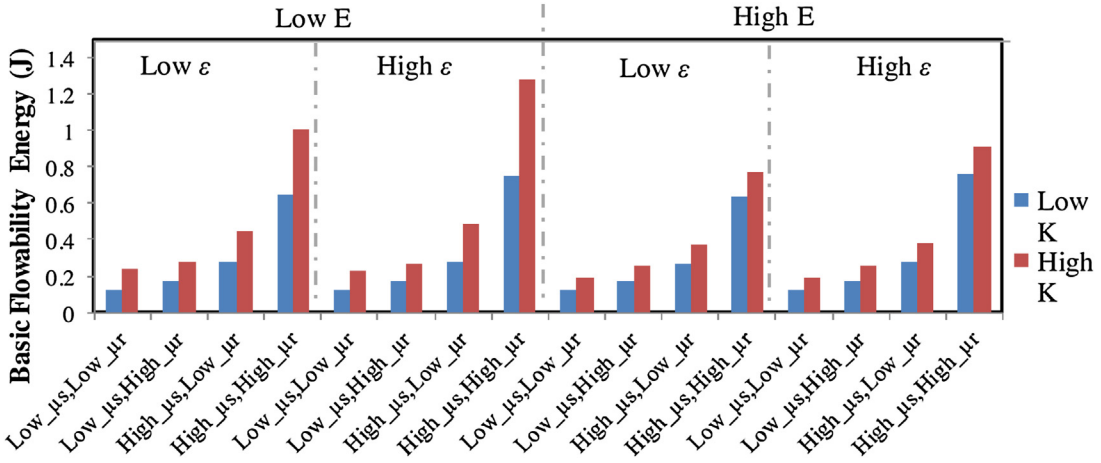

Fig. 7. Effect of cohesion energy density on flow energy.

3.3.5. *Effect of cohesion energy density*

Fig. 7 shows the effect of the cohesion energy density on the flow energy measurement, whereby for the same input parameters, high cohesion energy density leads to high flow energy. Additionally, for the same level of cohesion energy density, lower Young's modulus causes higher flow energy. This implies that the Young's modulus and cohesion energy density are negatively cross correlated input parameters. For soft particles, the total particle-particle contact area is much larger than rigid particles; hence the contribution and the cohesion energy density can be significant.

From the above discussions, we are able to see the effect of input parameters and possible correlation between input parameters.

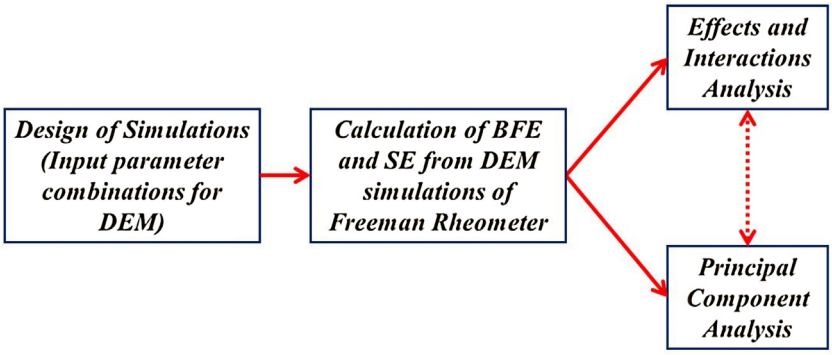

Fig. 8. Generalised flow diagram of approach to statistical and sensitivity analysis used in this study.

However, the results need to be interpreted many times to evaluate the effect of one input parameter at a time. What is more, it is not practical to look at the sensitivity of input parameters and the interactions between input parameters. This study employed more systematic and efficient statistical methods to look into both the input parameter sensitivity and cross-correlation between input parameters.

4. Statistical and sensitivity analysis

Fig. 8 details the overall approach applied to the statistical and sensitivity analysis in this study:

The calculated BFE and SE values from the simulations will be treated in three stages. Firstly, empirical 'effects and interactions' analysis will be carried out using the methods described in Sections 2.3.1 and 2.3.2. Empirical models will assess the importance of the five varied DEM input parameters (and interactions between them) on the BFE and SE model responses. The findings from this approach will then be compared to the PCA approach described in Section 2.3.2. The PCA approach involves the use of a matrix of input parameter values against model BFE and SE responses. A cross interpretation between these results will be carried out to understand the importance of the DEM input parameters in influencing calculated powder flow energies.

Additionally, both approaches will be assessed using different levels of DoS, such as full and half factorial. Here, the effectiveness of reduced factorial designs will be contrasted to the full factorial and recommendations on how effective these designs are will be discussed.

4.1. Effects and interactions analysis results

Empirical effects and interactions analysis was carried out using the following model as a starting point:

$$\begin{aligned} y(BFE \quad or \quad SE) &= \beta_1 + \mu_{s,pp}\cdot\beta_2 + \mu_{r,pp}\cdot\beta_3 \\ &+\varepsilon_p\cdot\beta_4 + Y\cdot\beta_5 + k\cdot\beta_6 + \mu_{s,pp}\cdot\mu_{r,pp}\cdot\beta_7 \\ &+\mu_{s,pp}\cdot\varepsilon_p\cdot\beta_8 + \mu_{s,pp}\cdot Y\cdot\beta_9 + \mu_{s,pp}\cdot k\cdot\beta_{10} \\ &+\mu_{r,pp}\cdot\varepsilon_p\cdot\beta_{11} + \mu_{r,pp}\cdot Y\cdot\beta_{12} + \mu_{r,pp}\cdot k\cdot\beta_{13} \\ &+\varepsilon_p\cdot Y\cdot\beta_{14} + \varepsilon_p\cdot k\cdot\beta_{15} + Y\cdot k\cdot\beta_{16} \end{aligned} \tag{14}$$

where,

- β_1 is an intercept fitting parameter to account for effects not described by the parameter effects or interactions in the system.
- $\beta_{2\text{-}6}$ are fitting parameters to account for the weighting magnitude of the effect the five DEM inputs parameters have on BFE or SE
- $\beta_{7\text{-}16}$ are fitting parameters to account for the weighting of the coupled interactions of the five DEM inputs parameters have on BFE or SE.

Table 4
Summary of significant effects and interactions for BFE empirical model.

Effect/Interaction	Design of Simulations		
	Full	Half	Qtr.
	Estimated Parameters (±95% Confidence Interval)		
Intercept	–	–	-0.37 ± 0.26
$\mu_{s,pp}$	0.25 ± 0.13	0.88 ± 0.35	0.77 ± 0.23
$\mu_{r,pp}$	–	–	0.52 ± 0.26
Y	$9.3 \pm 5.3\ (10^{-3})$	$1.3 \pm 0.4\ (10^{-2})$	$3.9 \pm 2.6\ (10^{-2})$
k	$7.4 \pm 3.2\ (10^{-2})$	–	–
$\mu_{s,pp}{}^{*}\mu_{r,pp}$	2.32 ± 0.33	2.21 ± 0.36	–
$\mu_{s,pp}{}^{*}Y$	–	$-6.6 \pm 3.6\ (10^{-2})$	–
$Y^{*}k$	$-6.8 \pm 3.5\ (10^{-2})$	–	–
Additional Information			
R^2 value	0.94	0.97	0.95
F-value[a]	120	144	35

[a] F-value for overall model significance. A value greater than $F_{crit} = 4.16$ implies the result is significant.

Table 4 details the significant parameter effects and interactions that were found to influence the calculated BFE. These parameters remained following use of the parameter reduction method described in Section 2.3.2. Examining the full factorial design result, the parameters $\mu_{s,pp}$, Y and k are all significant and have a positive correlation with BFE. The roles of $\mu_{s,pp}$ and k in hindering powder flowability is widely found in literature. Some literature shows Y has insignificant effect on the powder flowability (Lommen et al., 2014; Yan et al., 2015) of non-cohesive powder; however, in this current case of cohesive system, Y also has a positive effect in BFE, this may be due to its interaction from cohesivity. Future experiments should be carried out to elucidate this. The interaction of $\mu_{s,pp}$ *and* $\mu_{r,pp}$ is significant, and has the lowest 95% confidence interval as percentage of the estimated value. This significant relationship draws parallels with the calculation of torque in the DEM simulations utilises both of these parameters in its calculation (Eq. (3)). This would explain why $\mu_{r,pp}$ is only seen as an interaction with $\mu_{s,pp}$ and not as a sole effect. In all results, the contribution of torque to total BFE or SE was always approximately an order of magnitude greater than the contribution of force. Y and k also interact in a negatively correlated manner, suggesting increasingly stiff but cohesive particles reduce the BFE.

Similar information is observed for the half factorial design with the exception that information on the role of k is lost. In the quarter factorial design, only a 6 parameter model featuring the intercept and effects parameters can be tested, due to limited degrees of freedom afforded by the smaller (10 observations) dataset. $\mu_{r,pp}$ is

Table 5
Summary of significant effects and interactions for SE empirical model.

Effect/Interaction	Design of Simulations		
	Full	Half	Qtr.
	Estimated Parameters (±95% Confidence Interval)		
Intercept	$6.7 \pm 0.7\ (10^{-2})$	$7.3 \pm 1.0\ (10^{-2})$	–
$\mu_{s,pp}$	$3.6 \pm 2.2\ (10^{-2})$	$6.1 \pm 3.7\ (10^{-2})$	0.15 ± 0.05
$\mu_{r,pp}$	–	–	0.10 ± 0.06
Y	–	–	$5.3 \pm 2.4\ (10^{-3})$
k	$8.6 \pm 4.7\ (10^{-3})$	–	–
$\mu_{s,pp}{}^{*}\mu_{r,pp}$	0.35 ± 0.05	0.32 ± 0.09	–
$\mu_{s,pp}{}^{*}\varepsilon_p$	$4.8 \pm 2.4\ (10^{-2})$	$4.9 \pm 2.4\ (10^{-2})$	–
$Y^{*}k$	$-7.0 \pm 5.0\ (10^{-4})$	–	–
Additional Information			
R^2 value	0.96	0.94	0.89
F-value[a]	124	74	30

[a] F-value for overall model significance. A value greater than $F_{crit} = 4.16$ implies the result is significant.

found to be significant, which will act as an aliased representation of the $\mu_{s,pp}{}^{*}\mu_{r,pp}$ interaction parameter.

In Table 5, it is observed that there are similarities and differences in the key effects and interactions affecting SE, in comparison to BFE. $\mu_{s,pp}$ and its interaction with $\mu_{r,pp}$ is again important in both the full and half factorial designs, stressing the impact of the torque calculations in all flowability measurements. $Y^{*}k$ again negatively correlates with SE but upon a loss of information in the half factorial, all non $\mu_{s,pp}$ influenced effects and interactions are lost from the expression. The need for a fitted intercept value in the SE model suggests that there is an additional effect(s) influencing the flowability that is not encompassed by the five varied DEM input parameters.

Fig. 9A and B show the normalised norms of the Jacobian matrix, as described in Eq. (8), for both BFE and SE with each type of factorial design. In Fig. 9A, the results suggest that k is the most significant effect/interaction for the full factorial design, closely followed by $\mu_{s,pp}{}^{*}\mu_{r,pp}$ and $Y^{*}k$. The lack of a significant k effect and $Y^{*}k$ interaction in the half factorial design is therefore surprising, given its significance in the full factorial. This suggests that key information can be easily lost on the k parameter in reduced factorial designs. Conversely, all parameters containing $\mu_{s,pp}$ remain unchanged or improve in significance for the half factorial design, suggesting this parameter plays a strong role throughout the dataset. The intercept and Y interaction gain further significance in the quarter factorial design. This would suggest that these parameters are aliased effects masking the interactions that cannot be calculated with the quarter factorial design.

For the SE response in Fig. 9B, there is again a strong consistency in the roles of $\mu_{s,pp}{}^{*}\mu_{r,pp}$ and $\mu_{s,pp}$ in both the full and half factorial designs. The fitted intercept is dominant, suggesting that regardless of choice of combination of the five parameters, other effects (for example particle density) may play a significant role on the calculated SE.

The parity plots in Fig. 10 provide a visualisation of the quality of the empirical model prediction. A clear observation in both the BFE and SE plots, regardless of factorial design, is that the results fall into two distinct 'regions'. These are exclusively defined by $\mu_{s,pp}$. If this parameter is in its low position, the BFE and SE values are in the lower energy region. When the $\mu_{s,pp}$ parameter is in its mid or high position, a result in the higher energy region is returned.

The BFE parity plot in Fig. 10 shows a poor prediction of the high energy values. In the half factorial design in particular, the predicted values are seen to flatten over a significant range of different calculated energies. This suggests that some of the parameters have a non-linear relationship with calculated BFE, which cannot be characterised by a simple effects and interactions model. For

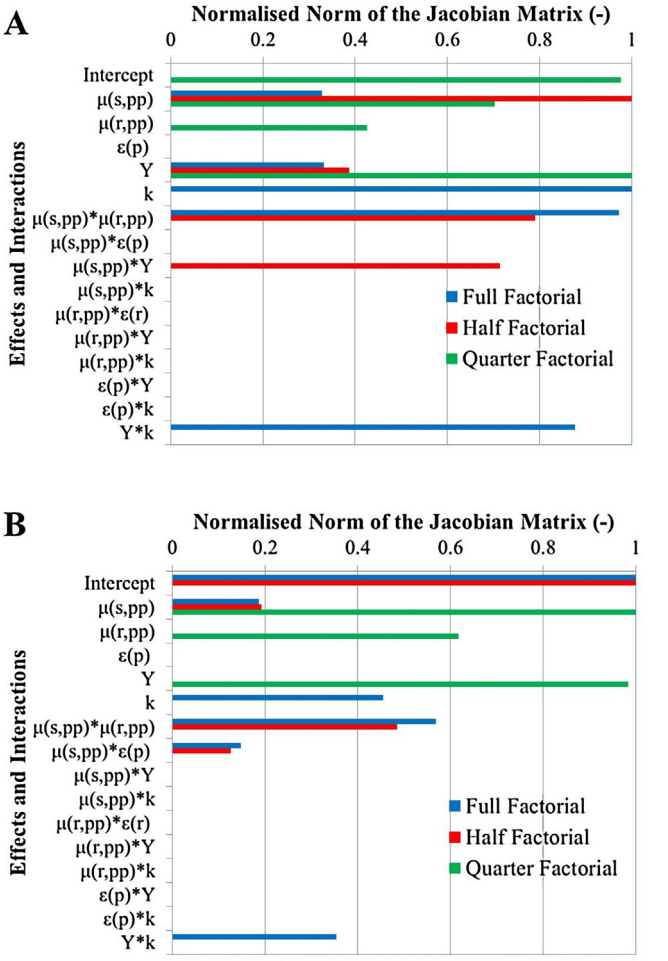

Fig. 9. Normalised norms of the Jacobian matrix for the final effects and interactions models for A) BFE and B) SE.

the SE calculation, this effect is less pronounced for the full factorial design but a clear prediction bias exists for the half factorial design, where less input information is available to the model.

In summary for the effects and interactions approach, both the BFE and SE datasets show strong indication that the $\mu_{s,pp}$ and $\mu_{s,pp}{}^{*}\mu_{r,pp}$ have a significant impact on the output energies of the simulation. The role of the other parameters however is less clear as the interpretations are strongly influenced by the choice of factorial design. Also the model results are not too differentiating between BFE and SE because of this; short of suggesting the user will gain understanding of the role of $\mu_{s,pp}$ from either test.

4.2. PCA results

Fig. 11 shows the PCA scores and loadings plotted as a biplot for both the full and half factorial datasets describing the BFE response:

Samples (coloured squares) that are similar to each other in multivariate space will be clustered together, and samples occupying opposite quadrants on the plots will show opposite behaviour. The same is true for the variables (black diamonds), in that variables which behave similarly (i.e., show correlation) will be close together, and will be opposite to anti-correlated variables in the plot. Samples and variables with the greatest contribution to the model, and hence to the model response variables, will be located at the outside of the plot.

A commonality between both the full and half factorial designs is that the first principal component (PC1), describing the greatest

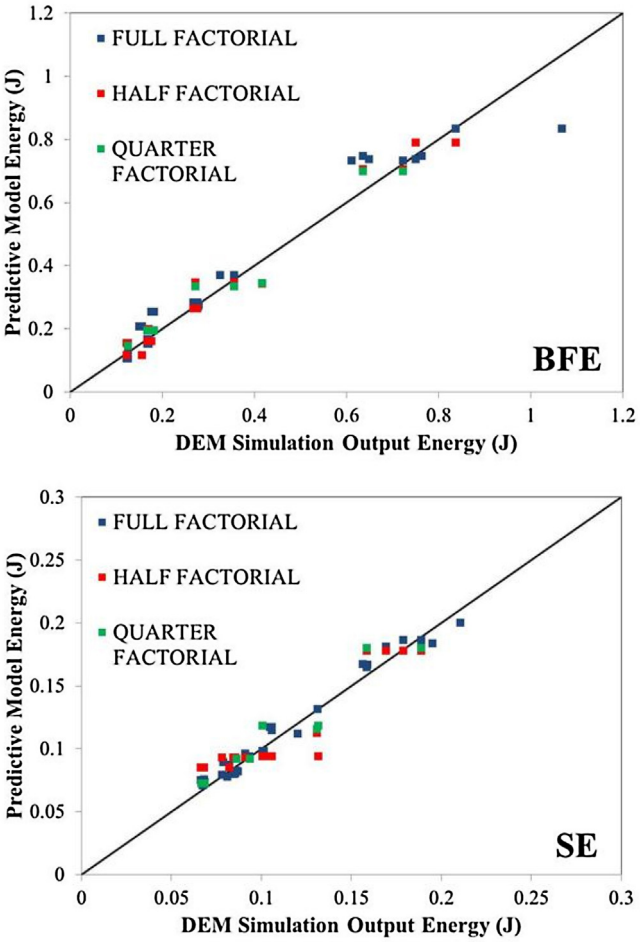

Fig. 10. Parity plots for predictive model vs. DEM simulation outputs for BFE and SE.

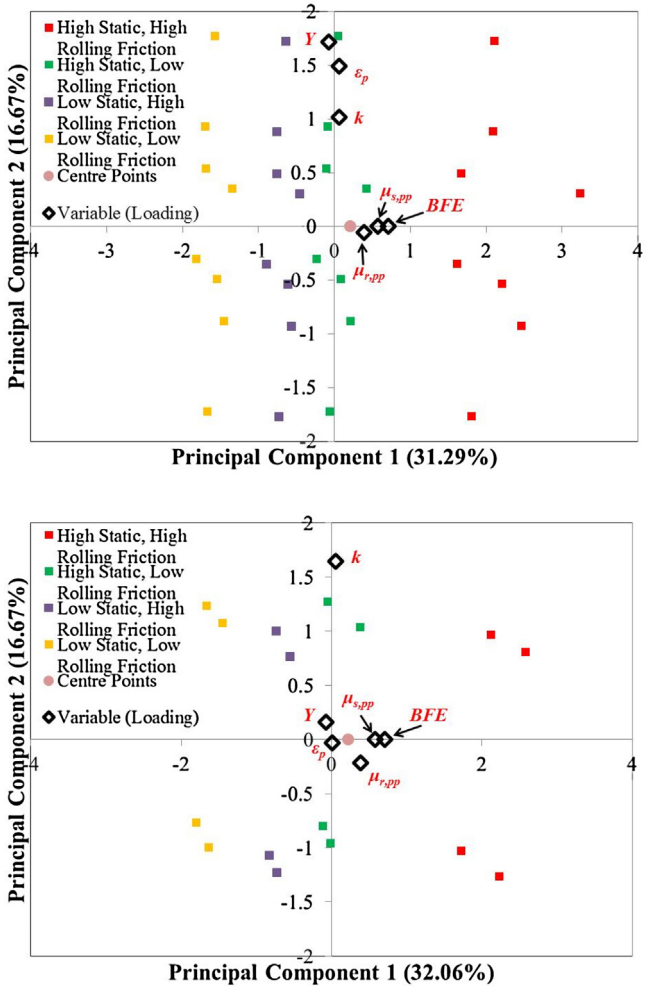

Fig. 11. PCA scores and loadings biplots for full (top) and half (bottom) factorial datasets for BFE.

variance in the system, is strongly differentiated by $\mu_{s,pp}$ and $\mu_{r,pp}$. Moving either of these parameters into its high position serves to increase the response value on PC1, which is matched by the positive loading of both of these parameters. The centre point holds a similar position to that of the high $\mu_{s,pp}$ and low $\mu_{r,pp}$ suggesting non-linearity in the system for these parameters.

The second principal component (PC2) shows a strong dependence on the remaining parameters ε_p, Y and k. The k parameter is still found to be significant in the half factorial design, suggesting that even when the amount of information on the system is reduced, an understanding of this parameter can still be ascertained. This is not the case for ε_{pp} and Y. Parameter k has a positive loading in both factorial designs, agreeing with the positive correlation seen in the effects and interactions analysis. PCA has provided greater clarity on the role of this parameter however by identifying its significance consistently.

In Fig. 12, the PCA for the SE response using the full factorial design shows a different relationship for $\mu_{s,pp}$ and $\mu_{r,pp}$ compared to the BFE response. Both have a positive loading with PC1 but also a positive ($\mu_{r,pp}$) and negative ($\mu_{s,pp}$) loading for PC2. This results in four distinct regions defined by low or high position of $\mu_{s,pp}$ and $\mu_{r,pp}$. The bi-directional influence of $\mu_{s,pp}$ may explain why the SE effects and interactions model contains an intercept term. Critically however, this difference in observation between the BFE and SE in the full factorial PCA presents an opportunity to differentiate $\mu_{s,pp}$ and $\mu_{r,pp}$ properties of a powder.

For the other parameters, only k is seen to have a significant loading in the half factorial design whilst they are insignificant in comparison to $\mu_{s,pp}$ and $\mu_{r,pp}$ in the full factorial design. This suggests that the information regarding k in the half factorial may relate to aliasing of the effect of $\mu_{s,pp}$ and $\mu_{r,pp}$ due to missing information in this design. Parameter k would be expected to feature in the full factorial in addition if it was truly a significant parameter. Hence this would suggest that only the BFE measurement would be expected to provide differentiation based on parameter k. For parameters Y and ε_p, little differentiation is afforded in either measurement.

4.3. Further discussion

The common theme between both the effects and interaction analysis and PCA is that $\mu_{s,pp}$ is a critical parameter influencing the simulated BFE and SE in the FT4. This echoes the findings in previous FT4 studies (Bharadwaj et al., 2010; Hare et al., 2015) and other DEM studies at large (Zhou et al., 2002; Yan et al., 2015). Additional commonalities with previous literature relate to the non-linearity of this parameter, with most significant changes being seen in the 0.05–0.25 value range. The interaction of the $\mu_{s,pp}$ and $\mu_{r,pp}$ parameters seen from both analysis methods in this work is a finding previously discussed to a much lesser degree. The link is logical, due to the influence that both parameters have on the torque calculations. This provides confidence that the empirical analysis in this paper provides a good reflection of fundamental particle behaviours with both parameters. The use of PCA is particularly

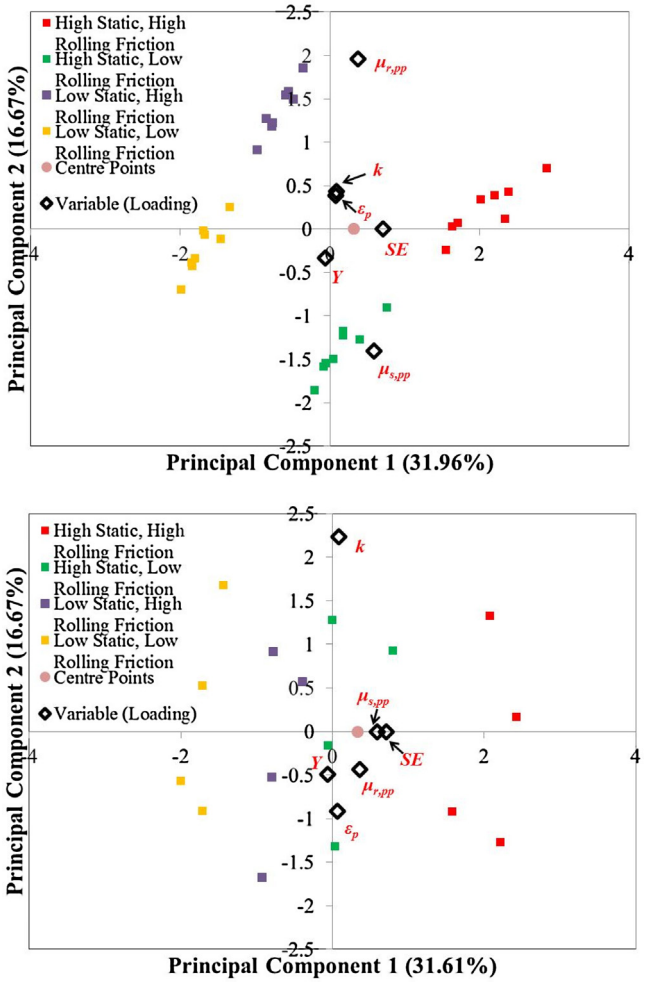

Fig. 12. PCA scores and loadings biplots for full (top) and half (bottom) factorial datasets for SE.

strong in differentiating the impact of both parameters in the BFE and SE test.

The role of energy of cohesion, *k*, has been much less clear in the FT4 literature. In the current work, it is seen that *k* remains dominant in extensive (full factorial) and reduced (half factorial) datasets for BFE measurements. In Freeman (2007), the BFE test was highly differentiating for non-cohesive powders but not for cohesive ones. This suggests that in the cohesive powder scenario the influence of *k* may also compete with frictional factors (represented *in silico* by $\mu_{s,pp}$ and $\mu_{r,pp}$ parameters), which are known to be significant, making experimental interpretation difficult. In a low *k* scenario, this competition is removed. Additionally, Freeman (2007) suggested a good correlation between experimental SE and shear strength measured using a shear cell. In the current DEM study, *Y* was found to be a weak parameter in the SE FT4 simulations. This might suggest that the $\mu_{s,pp}$ and $\mu_{r,pp}$ parameters, seen to be significant in the SE investigation in this study, may correlate with material shear strength. Additionally, it may relate to the fact that stress levels are low in the SE test, which would reduce the impact of Y.

The *Y* and ε_p parameters were found to be largely insignificant in influencing the outcome of the simulations. This suggests that these parameters cannot be adequately explored for a given powder using *in silico* FT4 simulations. This may relate to findings previously discussed in Yan et al. (2015). Both of these parameters were found to be strongly cross correlated in the underpinning contact force and torque models used in DEM. Furthermore, the use of sensitivity analysis in this study revealed those parameters to have a small influence on these models and ultimately on observed bulk powder responses in a sandpile test, such as hopper flow rate and angle of repose. Additionally, previous FT4 literature does not suggest these parameters to be significant in influencing simulation results (Bharadwaj et al., 2010; Hare et al., 2015). Alternative techniques such as the shear test and direct compression test have been employed to compare DEM simulations against experimental data (Coetzee and Els, 2009). This work revealed that different systems output for a given contact model will be dependent on different DEM input parameters. Shear test results were dependent on both the particle friction coefficient and the particle stiffness whereas the compression test was only dependent on the particle stiffness.

Previous literature has discussed the use of PCA (Boukouvala et al., 2013) and statistical design of experiments (Souihi et al., 2013) to improve interpretation of DEM simulations and understand key parameters. In this work, the combination of these approaches, with the addition of effects and interaction analysis, has allowed for a more robust interpretation in correlating bulk powder behaviour to DEM parameters. The $\mu_{s,pp}$ and $\mu_{r,pp}$ parameters have been shown to be significant irrespective of using PCA, effects and interactions analysis and reduced DoS matrices. The multi-approach framework has strengthened interpretation and has also given insight into the detail of understanding we get from different techniques. In this study, effects and interactions analysis gives a good first pass of system understanding but PCA can give much greater insight on which parameters drive primary and secondary effects in the system, as well as their influence in negatively or positively influencing the response.

5. Conclusions

In Section 1: Introduction, a number of aims were set out for the study; the outcomes from these are summarised below.

- *Understand the impact of particle property input parameters on measured flowability energies using DEM simulations of the FT4:* The impact of five particle property input parameters ($\mu_{s,pp}$, $\mu_{r,pp}$, ε_p, *Y*, *k*) on FT4 DEM simulations was assessed. Using BFE and SE as the measured responses variables, it was found that the coupling of $\mu_{s,pp}$ and $\mu_{r,pp}$ plays a major role on the measured output. This relates to the role which both parameters have in influencing torque response in the underpinning equations in DEM. In general, an increase of either parameter will result in a higher BFE or SE. The one exception here is for $\mu_{s,pp}$ for the SE response where a negative relationship was found with the second principle component in the PCA. It is also concluded that *k* plays a significant role in the outcomes of the BFE test, but less so in that for SE. *Y* and ε_p parameters both have a weak impact on the outcome of the FT4 simulations.
- *Recommend an approach that achieves the above understanding with an efficient number of simulations:* The use of design of simulations (DoS) has allowed a wide experimental space of DEM input parameters to be explored. A full factorial simulation design was tested as a benchmark (35 simulations) and comparisons were made with reduced half- (18 simulations) and quarter- (10 simulations) factorial designs. The use of reduced factorial designs can still provide clear insight into the key influential parameters on the system, namely $\mu_{s,pp}$ and $\mu_{r,pp}$, but care is needed in interpretation of secondary effects, such as *k*. In the SE response, its importance in the half factorial design is essentially an aliased effect. In conclusion, the DoS approach is recommended as a means to gain efficient model insight and the modeler should base a design on the extent of the factorial design based on the detail of understanding they require.

- *Recommend statistical and sensitivity analysis tools which can be combined to deliver a robust understanding of the impact of input parameters on the FT4 simulation:* The combination of empirical effects and interaction analysis with PCA has provided a complementary approach to deliver a robust understanding of FT4 behaviour. The effects and interactions approach a good first pass understanding of the system, and is able to describe the influence of the most sensitive parameters, namely $\mu_{s,pp}$, $\mu_{r,pp}$ and k. PCA is able to probe these findings in more detail and explore which of these parameters contribute to primary and secondary effects in the system. This provides a preference order of which parameters the user would be able to use calibrate using the FT4 system.
- *Discuss whether understanding from FT4 simulations in DEM can act as a (qualitative) road map and calibration tool for observations in experimental FT4 tests based on chosen powder properties the user wishes to measure. Discuss in which areas of powder processing the use of the FT4 may therefore significantly help in process design:* This *in silico* study has delivered a firm conclusion that the FT4 can be used as a calibration tool between powders which vary in rolling and static friction coefficients. The impact of these parameters would be seen in both a BFE and SE test. The SE test would act as the secondary differentiator here as the PCA results suggest there is a negatively correlated secondary effect as a function of static friction coefficient. The results also suggest that differentiation of cohesive and non-cohesive powders is possible through the BFE test, rather than the SE test. The final finding is that parameters Y and ε have a relatively weak influence on the system. Hence, the use of the FT4 as a characterisation tool for these parameters is not recommended. For powder handling processes which require a good understanding of these two parameters, alternative techniques such as direct compression for Y (Coetzee and Els, 2009) and direct impact tests for the coefficient of restitution ε (Radil and Palazzolo, 1994; Sand and Rosenkrantz, 2013; Hastie 2013).

Next steps for this direction of work fall into a number of areas. Firstly, in terms of assessing FT4 behaviour *in silico*, it would be prudent to further investigations into other parameters such as those concerning the interaction of the particles with the blade and wall. Additionally, factors such as aspect ratio, particle size and density should also be considered. Such factors may influence the "intercept" term observed in the effects and interactions analysis of the SE response. Another recommendation would be to look at the torque and contact force responses in more detail – this could either be as a final value which contributes to the BFE and SE calculation or to the transient data. Within the transient data, the impact of parameters on noise of the response could be a useful pursuit as this could be linked to real experimental observations.

For the DoS approach, an extension to improve this method would be to incorporate sequential simulation design methods following analysis of results of initial DoS. Such methods pick out the best 'next simulation' which can improve model understanding and could allow sparse experimental designs to be used as a start point for investigation. Additionally, the statistical and sensitivity analysis approaches should be applied to other processes and powder characterisation tools simulation in DEM.

A longer term goal for this work is in the translation of these findings into experimentation. In particular, a useful step would be to explore the impact of the key parameters identified in this study, as well as demonstrate the low impact of ε and Y identified by this work. Model materials could be selected for this purpose, however the requirements to undertake such a study will be extensive. Confident experimental measurement of intrinsic powder properties, so the Freeman rheometer experiment "input parameters" can be understood, is not straightforward.

An example of these difficulties is found in Samimi et al. (2005) which attempted to measure the Young's modulus of differently sized detergent granules from single granule compression tests. Estimates for 1.00–1.18 mm and 1.70–2.00 mm granules were $Y = 7.5 \pm 3$ and 10 ± 5 MPa respectively, which is a wide confidence range. Some parameters also exhibit strong interrelation in real materials, with the example of the weaker parameters ε and Y. This has been shown with first principles cross correlation analysis in Yan et al. (2015) but is also seen in studies of DEM speedup (Lommen et al. (2014)) and in studies of the impact of stiffness on particle overlap and simulation time step in DEM (Malone and Xu, (2008)). Given that high values of Y are typically accompanied by low values of ε in real practical materials, full deconvolution of the role of these parameters is challenging at best. A design of simulations in DEM affords broader exploration of these effects, even if impractical in real materials, to develop a more robust understanding of the impact of powder properties on powder flow. As such the authors expect that the findings in this study could guide experimental powder property discrimination in a qualitative sense in future applications.

Acknowledgment

This work is supported by the IPROCOM Marie Curie initial training network, funded through the People Programme (Marie Curie Actions) of the European Union's Seventh Framework Programme FP7/2007-2013/under REA grant agreement No. 316555.

Appendix A. Supplementary data

Supplementary data associated with this article can be found, in the online version, at http://dx.doi.org/10.1016/j.compchemeng.2016.11.034.

References

Alizadeh, E., Bertrand, F., Chaouki, J., 2014. Discrete element simulation of particle mixing and segregation in a tetrapodal blender. Comp. Chem. Eng. 64, 1–12.
Anand, A., Curtis, J.S., Wassgren, C.R., Hancock, B.C., Ketterhagen, W.R., 2008. Predicting discharge dynamics from a rectangular hopper using the discrete element method (DEM). Chem. Eng. Sci. 63 (24), 5821–5830.
Benvenuti, L., Kloss, C., Pirker, S., 2016. Identification of DEM simulation parameters by artificial neural networks and bulk experiments. Powder Technol. 291, 456–465.
Bharadwaj, R., Ketterhagen, W.R., Hancock, B.C., 2010. Discrete element simulation study of a Freeman powder rheometer. Chem. Eng. Sci. 65, 5747–5756.
Boukouvala, F., Gao, Y., Muzzio, F., Ierapetritou, M.G., 2013. Reduced-order discrete element method modelling. Chem. Eng. Sci. 95, 12–26.
Cleary, P.W., Sawley, M.L., 2003. DEM modelling of industrial granular flows: 3D case studies and the effect of particle shape on hopper discharge. App. Math. Model. 26 (2), 89–111.
Coetzee, C.J., Els, D., 2009. Calibration of discrete element parameters and the modelling of silo discharge and bucket filling. Comput. Electron. Agric. 65 (2), 198–212.
Cundall, P.A., Strack, O.D.L., 1979. A discrete numerical model for granular assemblies. Geotechnique 29 (1), 47–65.
Davies, M., Brindley, A., Chen, X., Marlow, M., Doughty, S.W., Shrubb, I., Roberts, C.J., 2005. Characterization of drug particle surface energetics and Young's modulus by atomic force microscopy and inverse gas chromatography. Pharm. Res. 22 (7), 1158–1166.
Dutt, M., Hancock, B.C., Bentham, A.C., Elliott, J.A., 2005. An implementation of granular dynamics for simulating frictional elastic particles based on the DL-POLY code. Comp. Phys. Comm. 166, 26–44.
Freeman, R., 2007. Measuring the flow properties of consolidated, conditioned and aerated powders – a comparative study using a powder rheometer and a rotational shear cell. Powder Technol. 174, 25–33.
Freireich, B., Litster, J., Wassgren, C., 2009. Using the discrete element method to predict collision scale behaviour: a sensitivity analysis. Chem. Eng. Sci. 64, 3407–3416.
Ganesan, V., Rosentrater, K.A., Muthukumarappan, K., 2008. Flowability and handling characteristics of bulk solids and powders – a review with implications for DDGS. Biosyst. Eng. 101, 425–435.
Grima, A.P., Wypych, P.W., 2011. Investigation into calibration of discrete element model parameters for scale-up and validation of particle-structure under impact conditions. Powder Technol. 212, 198–209.

Guo, Y., Wu, C.Y., Kafui, K.D., Thornton, C., 2010. Numerical analysis of density-induced segregation during die filling. Powder Technol. 197 (1–2), 111–119.
Höhner, D., Wirtz, S., Scherer, V., 2013. A study on the influence of particle shape and shape approximation on particle mechanics in a rotating drum using the discrete element method. Powder Technol. 278, 286–305.
Hare, C., Zafar, U., Ghadiri, M., Freeman, T., Clayton, J., Murtagh, M.J., 2015. Analysis of the dynamics of the FT4 powder rheometer. Powder Technol. (in press).
Hassanpour, A., Ghadiri, M., 2004. Distinct element analysis and experimental evaluation of the Heckel analysis of bulk powder compression. Powder Technol. 141 (3), 251–261.
Hastie, D.B., 2013. Experimental measurement of the coefficient of restitution of irregular shaped particles impacting on horizontal surfaces. Chem. Eng. Sci. 101, 828–836.
Hertz, H., 1881. Ueber die Berührung fester elastischer Koerper. J. Reine Angew. Math. 92, 156–171.
Johnson, K.L., Kendall, K., Roberts, A.D., 1971. Surface energy and the contact of elastic solids. Proc. R. Soc. Lond. A: Math. Phys. Eng. Sci. 324 (1558), The Royal Society, 1971.
Jolliffe, I., 2002. Principle Component Analysis. John Wiley and Sons Ltd.
Jones, R., 2003. From single particle AFM studies of adhesion and friction to bulk flow: forging the links. Gran. Matter. 4 (4), 191–204.
Ketterhagen, W.R., Curtis, J.S., Wassgren, C.R., Hancock, B.C., 2009. Predicting the flow mode from hoppers using the discrete element method. Powder Technol. 195 (1), 1–10.
Kloss, C., Goniva, C., Hager, A., Amberger, S., Pirker, S., 2012. Models, algorithms and validation for opensource DEM and CFD-DEM. Prog. Comput. Fluid Dyn. Int. J. 12 (2), 140–152.
Leisena, D., Kerkamma, I., Bohna, E., Kamlah, M., 2012. A novel and simple approach for characterizing the Young's modulus of single particles in a soft matrix by nanoindentation. J. Mater. Res. 27 (24), 3073–3082.
Liu, L., Kafui, K.D., Thornton, C., 2010. Impact breakage of spherical, cuboidal and cylindrical agglomerates. Powder Technol. 199 (2), 89–196.
Liu, S.D., Zhou, Z.Y., Zou, R.P., Pinson, D., Yu, A.B., 2014. Flow characteristics and discharge rate of ellipsoidal particles in a flat bottom hopper. Powder Technol. 253, 70–79.
Lommen, S., Schott, D., Lodewijks, G., 2014. DEM speedup: stiffness effects on behaviour of bulk material. Particuology 12, 107–112.
Malone, K.F., Xu, B.H., 2008. Determination of contact parameters for discrete element method simulations of granular systems. Particuology 6, 521–528.
Marigo, M., Stitt, E.H., 2015. Discrete element method (DEM) for industrial applications: comments on calibration and validation for the modelling of cylindrical pellets. KONA Powder Part. J. 32, 236–252.
Marigo, M., Cairns, D.L., Davies, M., Cook, M., Ingram, A., Stitt, E.H., 2010. Developing mechanistic understanding of granular behaviour in complex moving geometry using the discrete element method. part A: measurement and reconstruction of turbula mixer motion using positron emission particle tracking. Comp. Mod. Eng. Sci. 59 (3), 217–238.
Marigo, M., Cairns, D.L., Bowen, J., Ingram, A., Stitt, E.H., 2014. Relationship between single and bulk mechanical properties for zeolite ZSM5 spray-dried particles. Particuology 14, 130–138.
Markauskas, D., Kacianauskas, R., 2006. Compacting of particles for biaxial compression test by discrete element method. J. Civ. Eng. Manag. 12 (2), 153–161.
Martin, C.L., Bouvard, D., 2003. Study of the cold compaction of composite powders by the discrete element method. Acta Mater. 51 (2), 373–386.
Matuttis, H.G., Luding, S., Herrmann, H.J., 2000. Discrete element simulations of dense packings and heaps made of spherical and non-spherical particles. Powder Tech. 109 (1–3), 278–292.
Mindlin, R.D., 1949. Compliance of elastic bodies in contact. ASME Trans. J. App Mech. 16, 259–268.
Mort, P., Michaels, J.N., Behringer, R.P., Campbell, C.S., Kondic, L., Kheiripour-Langroudi, M., Shattuck, M., Tang, J., Tardos, G.I., Wassgren, C., 2015. Dense granular flow – a collaborative study. Powder Technol. 284, 571–584.
Moysey, P.A., Thompson, M.R., 2005. Modelling the solids inflow and solids conveying of single-screw extruders using the discrete element method. Powder Technol. 153 (2), 95–107.
Nasato, D.S., Goniva, C., Pirker, S., Kloss, C., 2015. Coarse graining for large-scale DEM simulations of particle flow – an investigation on contact and cohesion models. Procedia Eng. 102, 1484–1490.
Owen, P.J., Cleary, P.W., 2009. Prediction of screw conveyor performance using the Discrete Element Method (DEM). Powder Technol. 193 (3), 274–288.
Pantaleev, S., Yordanova, S., Ooi, J., Marigo, M., 2015. Powder mixing – an experimentally validated DEM study. In: Joint 5th UK-China & 13th UK Particle Technology Forum, 13rd-15th 2015, Leeds, UK.
Pearson, K., 1901. On lines and planes of closest fit to systems of points in space. Philos. Mag. Ser. 6 2 (11), 559–572.
Prabhu, B., 2005. Microstructural and Mechanical Characterization of Al-Al_2O_3 Nanocomposites Synthesized by High-Energy Milling. Dissertation University of Central Florida, Orlando.
Quiney, A.S., Schuurman, Y., 2007. Kinetic modelling of CO conversion over a Cu/ceria catalyst. Chem. Eng. Sci. 62, 5026–5032.
Radil, K.C., Palazzolo, A.B., 1994. Influence of temperature and impact of velocity on coefficient of restitution. NASA Tech. Memo., 106485.
Radl, S., Radeke, C., Khinast, J.G., Sundaresan, S., 2011. Parcel based approach for the simulation of gas particle flows. In: 8th Int Conference on CFD in Oil and Gas, Trondheim, Norway.
Remy, B., Canty, T.M., Khinast, J.G., Glasser, B.J., 2010. Experiments and simulations of cohesionless particles with varying roughness in a bladed mixer. Chem. Eng. Sci. 65, 4557–4571.
Samimi, A., Hassanpour, A., Ghadiri, M., 2005. Single and bulk compressions of soft granules: experimental study and DEM evaluation. Chem. Eng. Sci. 60 (14), 3993–4004.
Sand, A., Rosenkrantz, J., 2013. Multiple criteria approach to model calibration in DEM simulation of compaction processes. In: SME Annual Meeting, Denver Colorado.
Simons, T.A.H., Weiler, R., Strege, S., Bensmann, S., Schilling, M., Kwade, A., 2015. A ring shear teste das calibration experiment for DEM simulations in agitated mixers – a sensitivity study. Procedia Eng. 102, 741–748.
Souihi, N., Josefson, M., Tajarobi, P., Gurarajan, B., Tyrgg, J., 2013. Design space estimation of the roller compaction process. Ind. Eng. Chem. Res. 52, 12408–12419.
Thakur, S.C., Ooi, J.Y., Ahmadian, H., 2015. Scaling of discrete element model parameters for cohesionless and cohesive solid. Powder Technol. (in press).
Thornton, C., Randall, C.W., 1988. Applications of theoretical contact mechanics to solid particle system simulation. In: Satake, M., Jenkins, T.J. (Eds.), Micromechanics Granular Matters. Eisevier, Amsterdam, pp. 133–142.
Thornton, C., Yin, K.K., Adams, M.J., 1996. Numerical simulation of the impact fracture and fragmentation of agglomerates. J. Phys. D. Appl. Phys. 29 (2), 424–435.
Wilkinson, S.K., McManus, I., Daly, H., Thompson, J.M., Hardacre, C., Sedaie Bonab, N., ten Dam, J., Simmons, M.J.H., D'Agostino, C., McGregor, J., Gladden, L.F., Stitt, E.H., 2015. A kinetic analysis methodology to elucidate the roles of metal, support and solvent for the hydrogenation of 4-phenyl-2-butanono over Pt/TiO_2. J. Catal. 330, 362–373.
Wu, C.Y., 2008. DEM simulations of die filling during pharmaceutical tableting. Particuology 6 (6), 412–418.
Yan, Z., Wilkinson, S.K., Stitt, E.H., Marigo, M., 2015. Discrete element modelling (DEM) input parameters: understanding their impact on model predictions using statistical analysis. Comp. Part. Mech., 56.
Yang, S., Evans, J.R.G., 2007. Metering and dispensing of powder; the quest for new solid freeforming techniques. Powder Technol. 178, 56–72.
Yang, R.Y., Yu, A.B., McElroy, L., Bao, J., 2008. Numerical simulation of particle dynamics in different flow regimes in a rotating drum. Powder Technol. 188 (2), 170–177.
Zhang, Z.P., Liu, L.F., Yuan, Y.D., Yu, A.B., 2001. A simulation study of the effects of dynamic variables on the packing of spheres. Powder Technol. 116 (3), 23–32.
Zhou, Y.C., Xu, B.H., Yu, A.B., Zulli, P., 2002. An experimental and numerical study of the angle of repose of coarse spheres. Powder Technol. 125, 45–54.